11

Shipton, Z. K., J. P. Evans, and L. B. Thompson, 2005, The geometry and thickness of deformation-band fault core and its influence on sealing characteristics of deformation-band fault zones, *in* R. Sorkhabi and Y. Tsuji, eds., Faults, fluid flow, and petroleum traps: AAPG Memoir 85, p. 181–195.

The Geometry and Thickness of Deformation-band Fault Core and its Influence on Sealing Characteristics of Deformation-band Fault Zones

Z. K. Shipton[1]

Department of Geology, Trinity College, Dublin 2, Ireland

J. P. Evans

Department of Geology and UF3-Innovation Campus, Utah State University, Logan, Utah, U.S.A.

L. B. Thompson

UF3, Innovation Campus, Utah State University, Logan, Utah, U.S.A.

ABSTRACT

Deformation-band faults in high-porosity reservoir sandstones commonly contain a fault core of intensely crushed rock surrounding the main slip surfaces. The fault core has a substantially reduced porosity and permeability with respect to both the host rock and individual deformation bands. Although fault core thickness is a large uncertainty in calculations of transmissibility multipliers used to represent faults in single-phase reservoir flow models, few data exist on fault core thickness in deformation-band fault zones. To provide accurate estimates of deformation-band fault petrophysical properties, we measured fault core thickness at six sites (each 4–15 m [13–49 ft] along strike) along the Big Hole fault in the Navajo Sandstone, central Utah. These data show that the thickness is highly variable and does not correlate with either the amount of slip or the number of slip surfaces. The thickness of the fault core is likely to be dependent on local growth processes, specifically the linkage of fault segments. This suggests that correlations of fault permeability with throw may not apply to deformation-band faults. Simple calculations of two-phase flow properties based on measured porosity and permeability values suggest that deformation-band faults

[1]*Present address:* Division of Earth Sciences, Centre for Geoscience, University of Glasgow, Glasgow, Scotland.

DOI:10.1306/1033723M853135

containing fault core are likely barriers to two-phase flow. More data on the variability of fault core thickness and its petrophysical properties need to be collected to characterize population statistics for models of deformation-band fault fluid-flow properties.

INTRODUCTION

Deformation bands are the dominant deformation elements in high-porosity sandstone (Aydin and Johnson, 1978). Deformation bands are zones of cataclasis commonly of the order of 1 mm (0.04 in.) thick, which accommodate offsets of less than a few millimeters. Increasing offset is accommodated by the progressive addition of deformation bands to form zones of bands, with offsets roughly proportional to the number of bands in the zone (Mair et al., 2000). Larger offsets are accommodated by throughgoing slip surfaces. In the model of Aydin and Johnson (1978), the evolution of deformation-band faults proceeds from the accumulation of single deformation bands to a cluster of deformation bands and to the presence of a slip surface. The Aydin and Johnston model does not address the process of slip-surface nucleation and propagation. Shipton and Cowie (2001) identified the fault core as a distinct deformation element in faults in the Navajo Sandstone, Utah, which continues to develop after the appearance of a throughgoing slip surface. The fault core consists of a narrow zone of intense cataclasis, accompanied by one or more slip surfaces. This fault core is surrounded by a damage zone consisting of deformation bands with occasional short segments of slip surfaces. This chapter presents preliminary data on the geometry and thickness of the fault core, their controlling growth processes, and their effect on the fluid-flow properties of deformation-band faults.

Deformation-band faults have been studied intensively in terms of their microstructures, fault geometries, petrophysical properties, influence on fluid flow, and their impact on the hydrocarbon industry (e.g., Pittman, 1981; Edwards et al., 1993; Antonellini and Aydin, 1994, 1995; Beach et al., 1997; Fisher and Knipe, 1998, 2001; Hesthammer et al., 2000; Jourde et al., 2002). They produce an order of magnitude or greater reduction of porosity and permeability with respect to the host rock. Shipton and Cowie (2001) showed that isolated deformation bands in the Navajo Sandstone (porosity 20–25%), Utah, have porosities of 3–13%, and the fault core has porosities as low as 1%. Antonellini and Aydin (1994) measured permeability values as low as 0.007 md adjacent to slip surfaces in the Entrada Sandstone, Utah. Deformation-band faults can therefore have a significant effect on fluid flow (Edwards et al., 1993; Knott, 1993; Gibson, 1994; Beach et al., 1997; Matthai et al., 1998; Antonellini et al., 1999; Fisher and Knipe, 2001; Ogilvie and Glover, 2001; Shipton et al., 2002).

Simple modeling of fluid flow in faults comprising clusters of deformation bands including a fault core allows the effect of varying parameters on the bulk permeability of the fault zone to be assessed (Shipton et al., 2002). Assuming that all fault elements are parallel, the bulk permeability is calculated in directions parallel and perpendicular to the fault using the weighted arithmetic mean and weighted harmonic mean, respectively. Sensitivity analyses of this fault model show that the thickness of the fault core is, by far, the most important variable for bulk fault zone permeability (Shipton et al., 2002). Therefore, the lack of data on fault core petrophysical properties and architecture makes it difficult to predict the permeability of deformation-band fault zones and to calculate representative transmissibility multipliers for use in reservoir models.

Most reservoir simulators represent faults as a transmissibility multiplier, T, assigned to the face of grid blocks that separate either side of the fault (Manzocchi et al., 1999). This assumes that the variability of fault zone properties can be upscaled to a homogenous effective value at the grid block scale. Determining appropriate values of T to assign across a fault surface is the focus of much research (Heinemann et al., 1998; Walsh et al., 1998; Manzocchi et al., 1999), but few geologic data exist that address how fault zone permeability or transmissibility varies along a fault plane. Most transmissibility values are assigned by a history-matching process (Heinemann et al., 1998). It would be preferable to make a physically based prediction of the transmissibility distribution on the fault surface prior to the start of production. Such analyses are critical, because in some cases, faults with transmissibility multipliers of less than 0.001 may retard fluid flow (Damsleth et al., 1998).

We examined the geometry, dimensions, and microstructures of fault core along the well-exposed Big Hole fault in the high-porosity Navajo Sandstone. The damage zone geometry of the Big Hole fault has been previously described in detail (Shipton and Cowie, 2001; Shipton et al., 2002), making it an ideal location for a study of fault core geometry and growth processes. Samples of fault core were collected for microstructural analysis at intervals along the fault zone with known displacement. We measured fault core thickness along the surface trace of the fault at several locations to characterize its spatial variability and its relationship to fault throw. We used these data to calculate likely permeability and capillary pressure values for the fault we measured. These data provide constraints on models of fluid flow in faults in high-porosity sandstones. We

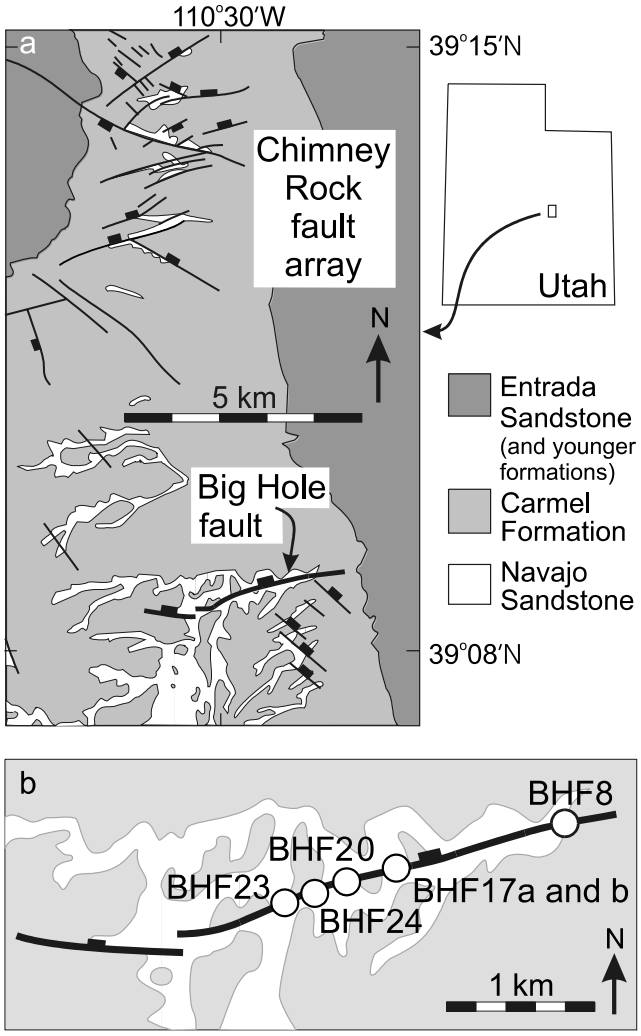

FIGURE 1. (a) Map of the Chimney Rock normal fault array showing the location of the Big Hole fault (BMF). Ticks mark the downthrown side of the faults. (b) Location of the survey sites along the Big Hole fault. Each site is referred to by the displacement on the main fault at that point, so BHF20 is the site at which the fault has 20 m (66 ft) displacement.

discuss flow parameters for faults in a specific setting and with a defined deformation mechanism (cataclasis in deformation bands). This approach has been successfully used elsewhere, for instance, in sheared-joint-based faults (Flodin et al., 2004) and clay-rich faults (Yielding et al., 1997).

GEOLOGICAL SETTING

The Big Hole fault is south of the Chimney Rock fault array in the northern San Rafael Swell, Utah (Figure 1). The faults are likely Late Cretaceous to early Tertiary in age, suggesting that faulting occurred under a lithostatic load of 40–80 MPa and temperatures of 75–90°C (Shipton and Cowie, 2001). Fault trace lengths range from 100 m (330 ft) to 4 km (2.5 mi), with displacements ranging up to 30 m (100 ft) (Krantz, 1988). Fault intersections in the Chimney Rock fault array create compartments of relatively undeformed host rock in the Navajo Sandstone (Figure 1), which are analogous to similar oil field- and aquifer-scale structures in porous sandstone (i.e., Gibson, 1994; Antonellini et al., 1999; Fossen and Hesthammer, 2000).

The faults cut the Jurassic Navajo Sandstone, a planar to cross-bedded, very fine- to fine-grained eolian arenite with about 90–95% quartz, 1–6% feldspar, and 1–3% clays. At this locality, the Navajo Sandstone is friable and weakly cemented by very low volumes of quartz overgrowths, iron oxide cements, and/or calcite cement. Primary porosity ranges from 13 to 25% (Shipton and Cowie, 2001). Permeabilities to water for the undeformed Navajo Sandstone, measured at room temperatures and pressures, are typically in the 100–1000-md range (Hood and Patterson, 1984) but can be greater than 4000 md (Shipton et al., 2002). Because of the relatively low volumes of cement in the host rock and the fault zone, we can investigate the mechanical aspects of fault sealing on fault-seal quality independently of the effects of diagenesis.

At the surface, the Big Hole fault strikes N70°E and dips 64°N with pure dip-slip slickenlines. Cowie and Shipton (1998) measured the fault throw from offset of the top Navajo Sandstone unconformity. A maximum of 29 m (95 ft) of throw at the fault center decreases approximately linearly toward each tip. The deeply incised, meandering Big Hole canyon provides sections through the fault zone structure. The fault typically consists of a fault core with one or more slip surfaces surrounded by clusters of deformation bands. The fault core sits in a damage zone consisting of deformation bands and occasional slip surfaces that are either synthetic or antithetic to the main fault.

FAULT CORE AND SLIP-SURFACE GEOMETRY

The fault core is a zone of fine-grained, pale-colored rock as much as 35 cm (14 in.) thick, bounded by or containing one or more slip surfaces (Figure 2). The fault core generally has a resistant, glassy, almost mylonitic appearance, although in thin section, it contains only cataclastic deformation (see next section). Occasionally, the fault core consists of a crumbly gouge (sample BHF24). Typically, several anastomosing slip-surface strands are present in the main fault zone. Slip surfaces are highly polished or mineralized and contain slickenlines. Both in outcrop and in drill core, these can be tightly mated surfaces (Figure 2a, b) or act as planes of parting (Figure 2c). Other slip surfaces that

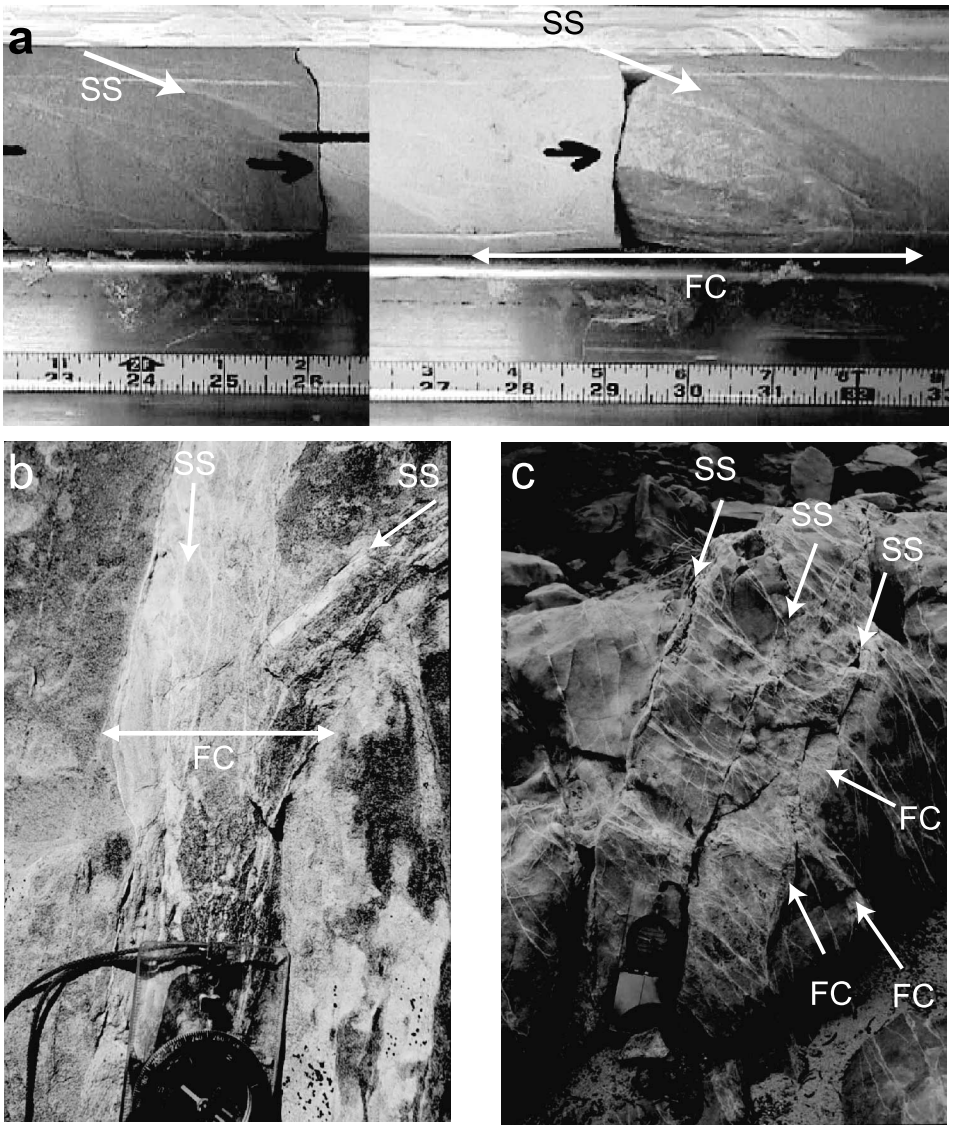

FIGURE 2. (a) Example of the fault core from a drill hole through the Big Hole fault at BHF17a (from Shipton et al., 2002). The fault core is a white zone of densely packed deformation bands and is bounded on either side by slip surfaces (SS). (b) Fault core from a subhorizontal outcrop of the Big Hole fault at BHF23. Note the anastomosing deformation bands in the fault core (FC) and the slip surface at the margins. (c) Slip surfaces in a zone of deformation bands away from the main fault. Note that these are planes of parting. Thin knots of fault core occur along these slip surfaces and are associated with a deformation-band cluster on the right side of the photo.

surround these throughgoing surfaces tip out in zones of deformation bands. Only the surface or surfaces that cut through the entire outcrop can be accommodating a substantial majority of the offset.

In plan view, the throughgoing slip surface of the main fault plane is decorated with elongated pods of fault core (Figure 3a). These lozenge-shaped pods are separated by areas with almost zero thickness of fault core. In cross section view, the fault core material is localized at intersections between synthetic and antithetic deformation-band clusters that contain slip surfaces (Figure 3b). Thus, the fault core can be visuaized in three dimensions as being thickest at the intersection of synthetic and antithetic deformation-band clusters that are not totally planar, producing pods in plan view. In deformation-band clusters away from the fault, the fault core can be developed (as much as 10 cm [4 in.] thick) without slip surfaces (Figures 2c, 3b). Thus, fault core can develop without large amounts of slip, and large-offset slip surfaces can develop without a large thickness of fault core. Throughgoing slip surfaces are always polished and can even look glassy, showing that a thin veneer of very fine-grained fault core material surrounds all the slip surfaces.

FAULT CORE MICROSTRUCTURES

To investigate the evolution of fault core and slip-surface microstructures with increasing displacement, oriented samples were collected from surface outcrops with a rock drill and from drill core. Thin sections were examined under an optical microscope and with cathodoluminescence (CL) and backscatter (BSEM) modes on an electron microscope. Thin sections of fault rock were oriented perpendicular to the fault plane and parallel to the slip vector.

The fault core is highly comminuted (Figures 4, 5), and relatively intact grains lie in a tightly packed matrix of angular crushed grains, with a low resulting porosity (Figure 4a). Some of these uncrushed grains have been planed off at individual slip surfaces (Figure 4b),

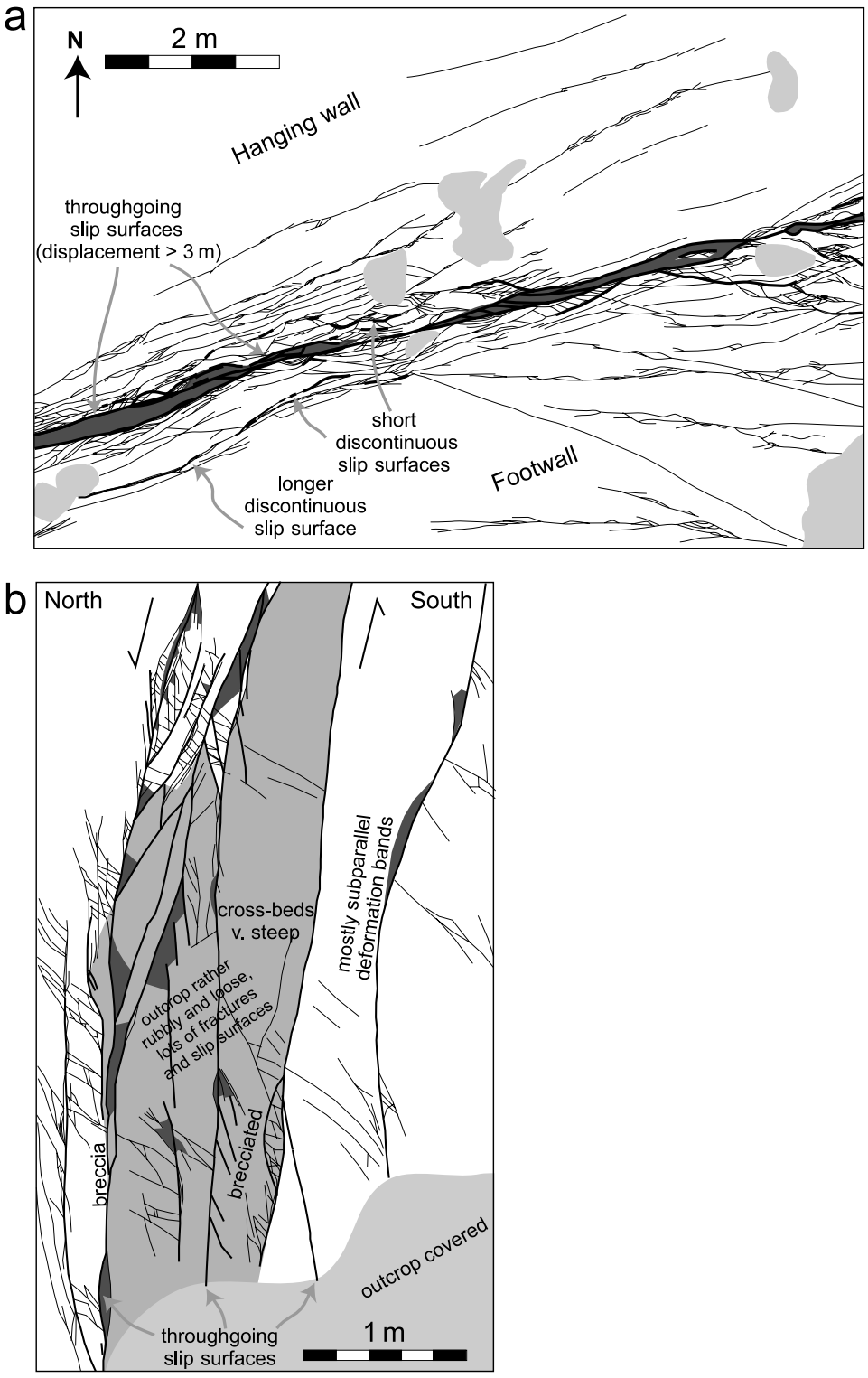

FIGURE 3. Fault core geometry. (a) Plan view of the outcrop at location BHF17. The fault core forms elongate lozenge-shaped pods (dark gray). Pale gray areas are sand on the outcrop. (b) Cross section view of a cliff outcrop at BHF23. Several slip surfaces cut the cliff face, and some can be seen to die out upward. Areas with very intense deformation, in which it is difficult to distinguish individual deformation bands, are shaded (medium gray). Some pods of breccia are marked. The fault core forms triangular areas at the intersection of synthetic and antithetic deformation band clusters (dark gray). A thin veneer of highly comminuted fault core material lines each of the slip surfaces but is too narrow to be represented on these figures.

indicating that transgranular fracturing is an important deformation mechanism along active slip surfaces. The fault core is therefore finer grained, with a larger variation in grain size than individual deformation bands. The thickness of the fault core can vary even on the scale of an individual thin section (Figure 4a). Aligned, unhealed transgranular microfractures are only seen in the zone of high grain crushing adjacent to the slip surfaces (Figure 4d). This is in contrast to microfractures in grains outside the fault core, which are rare and exclusively contained in individual grains.

Slip surfaces appear as thin (less than 1 mm [0.04 in.] thick), dark surfaces under plain polarized light. Under crossed polars, the areas of crushed grains, which surround all of the slip surfaces, become more apparent (Figure 4b). Slip surfaces can bifurcate and link at all angles, and wider zones of intense grain crushing are localized at the points where slip surfaces link (Figure 5a, b). Figure 5c shows two slip surfaces that curve toward one another. We interpret this as the interaction and propagation of two slip surfaces toward each other, and that therefore, the slip surfaces have propagated in the fault core.

Bands of highly comminuted grains occur in the fault core at an angle of 15° to the main fault (Figure 4a,b).

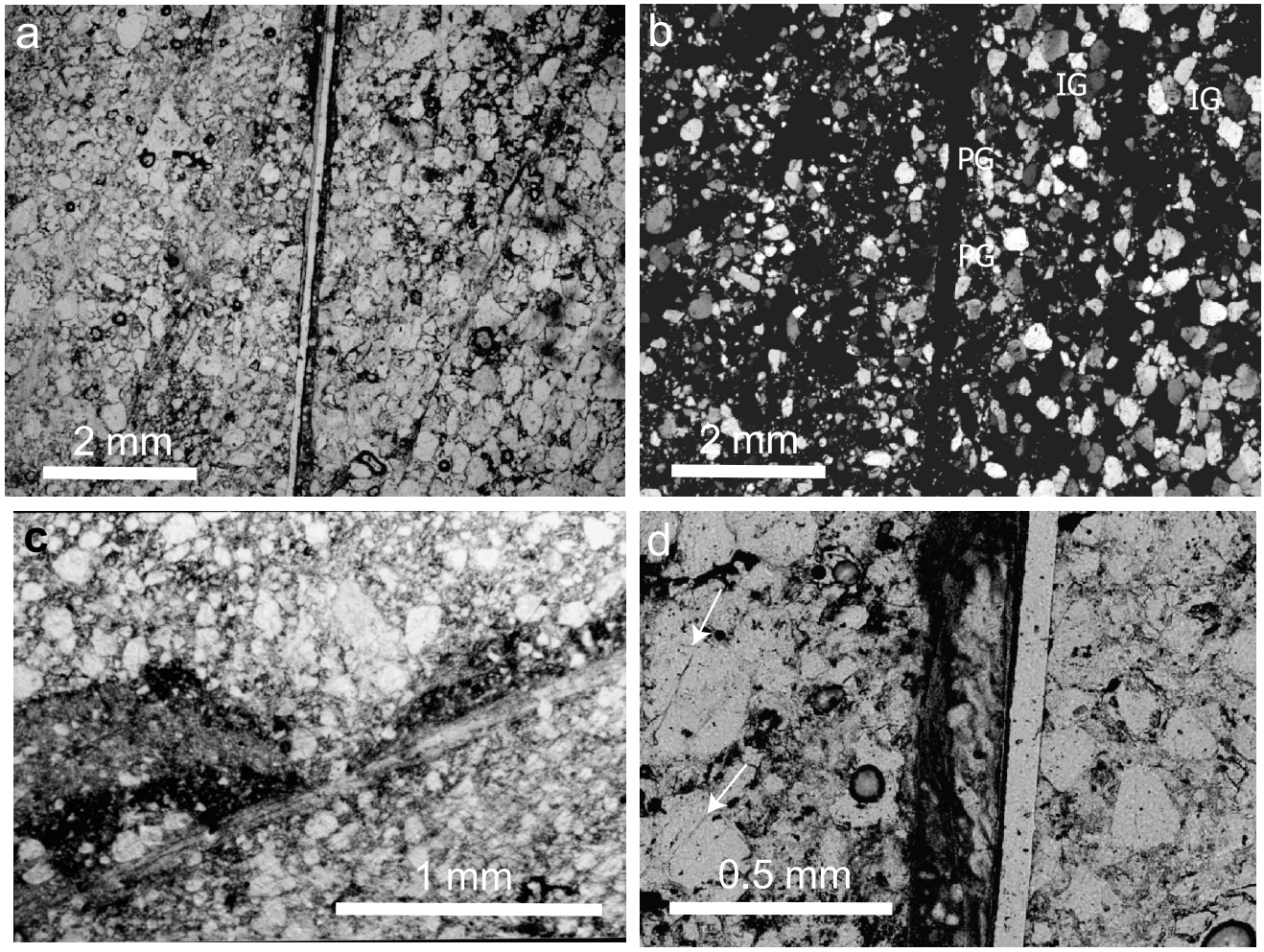

Figure 4. Photomicrographs of fault core microstructures. (a) Plane-polarized image and (b) crossed polars image of the main fault plane at BHF17. The highly crushed bands running at angles to the main fault are in the correct orientation to be Riedel shears formed in the progressively deforming crushed zone. IG marks indented grains formed by pressure solution. PG marks planed-off grains formed by transgranular fracture and movement along the slip surface. This slip surface parted during sample preparation. (c) Plane-polarized image of the fault from a drill core at displacement = 3 m (10 ft). Highly crushed material occurs all along the slip surface (pale, fine grained), but less-comminuted fault core material containing relatively intact grains surrounds this. The thickness of the fault core varies in thickness even on the scale of this thin section. Note that this material has been infiltrated by a dark cement adjacent to the slip surface. (d) Plane-polarized image of the main slip surface at BHF17 (just above a). The slip surface in this sample is not cemented, but note the dark, fine-grained cement in the fault core on the left side of the slip surface. In addition, note the microfractures in the grains on the left side of the image (arrowed).

These Riedel shearlike structures suggest that there has been some bulk movement in fault core material. The aligned microfractures and Riedel shears demonstrate a change in deformation mechanism from grain rolling and crushing in zones of deformation bands to brittle fracturing in the fault core. Grain crushing, microfracturing, and the formation of Riedel shears show that there has been bulk movement in the fault core after the nucleation of the slip surfaces and as further displacement is accumulated.

The traditional model for the growth of deformation-band faults suggests that a zone of deformation bands is a precursor to slip-surface development (Aydin and Johnson, 1978), but processes of slip-surface nucleation and growth are unclear from this model. Our observations suggest that the process of slip-surface growth is intimately linked with the growth and, therefore, geometry of the fault core. Understanding slip-surface growth is therefore crucial to predicting the likely variability of petrophysical properties across faults with sand-sand juxtapositions. Localized increase of granulation does occur in zones of deformation bands before slip-surface initiation, so grain crushing must be an early stage in the formation of slip surfaces. Shipton and Cowie (2001) noted that a high degree of grain crushing is seen ahead of fault tips where the slip surfaces

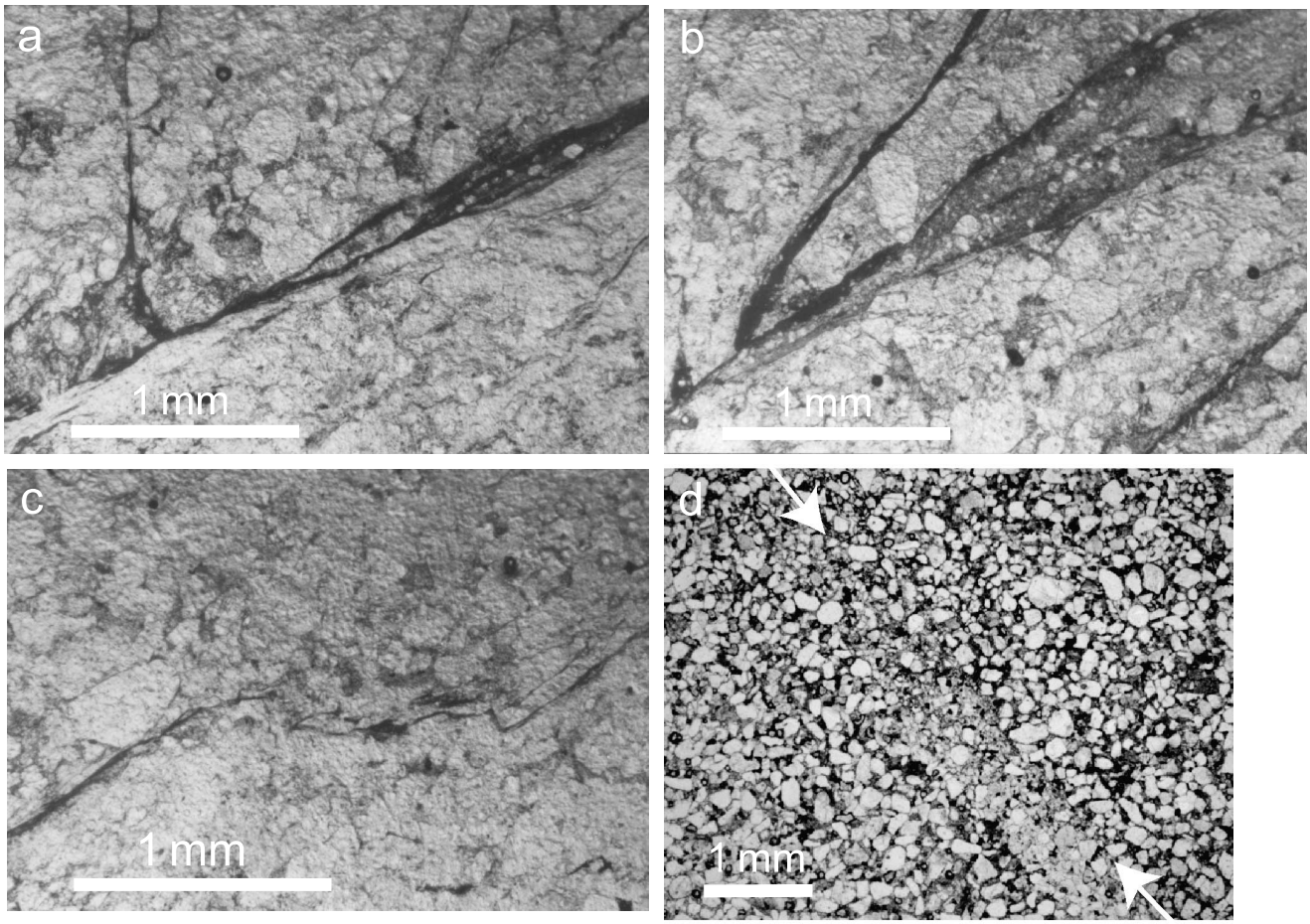

FIGURE 5. Plane polarized images of slip-surface geometries. (a) The main slip surface at BHF8. Surface bifurcates on the right side of the image. Note that the second slip surface joins at a high angle from the top. (b) Main fault plane slip surface at BHF8. Second slip surface joins at a lower angle from the top right, with increased grain crushing between these surfaces, forming a pod of fault core. (c) Linkage of two slip-surface segments away from the main fault slip surface at BHF8. Note how the slip surfaces are curving toward each other. Could further accumulation of displacement on this structure result in the formation of fault core material? (d) A surface in a deformation band cluster at BH20. Offset of eolian cross-beds in the Navajo Sandstone shows that this surface has accommodated 5 cm (2 in.) of slip. The grain crushing is more intense at the top of this deformation band (shown by the arrows). This region has the straight edges characteristic of slip surfaces. Is this a slip surface in the making?

are poorly developed (their figure 11). However, the development of fault core continues after the formation of a throughgoing surface.

EVIDENCE FOR FLUID FLOW IN THE FAULT CORE AND SLIP SURFACES

The fine-grained fault core is likely to be a barrier to fluid flow (Antonellini and Aydin, 1994; Shipton et al., 2002), but the permeability of slip surfaces is more complex. Slip surfaces can be either closely mated (Figure 2a) or planes of parting (Figure 2c), in both outcrop and drill core. The aperture of the slip surfaces is not simply related to surface weathering, and slip surfaces can have high along-fault permeability at depth. The reduction of porosity and permeability in deformation bands and fault core suggests that they would affect fluid flow through the highly porous Navajo Sandstone. However, cement (barite and oxides) is commonly localized along slip surfaces and in places has penetrated into the fault core (Figure 4c). These cements are sparse elsewhere in the deformation-band faults or host rock. Indented grain boundaries show that pressure solution has been active (Figure 4b). From CL observations, it can be seen that some fractured grains have been cemented with quartz after crushing, giving rise

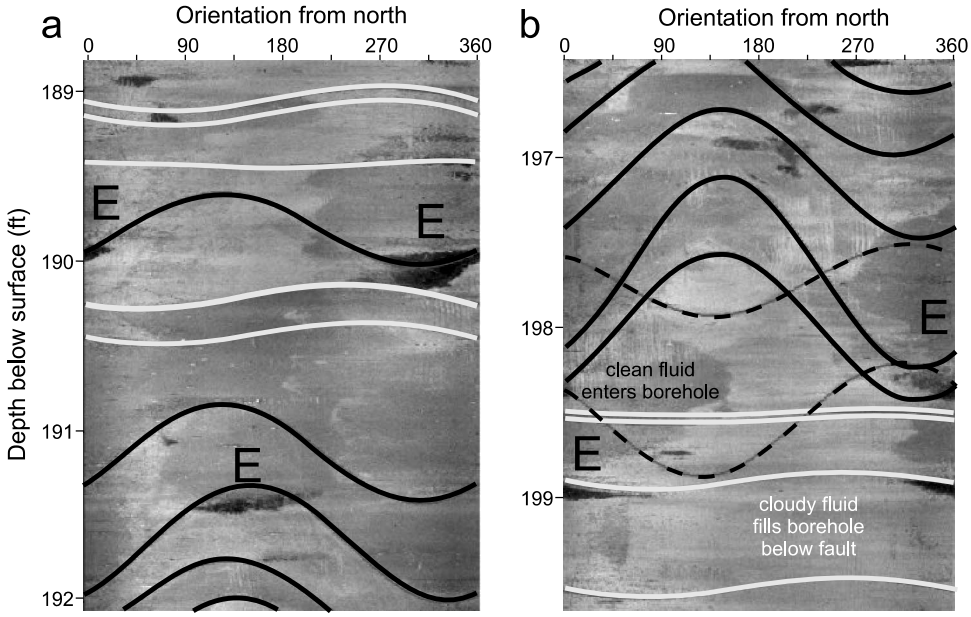

FIGURE 6. Downhole video image logs of a borehole drilled through the Big Hole fault where the displacement = 5 m (16 ft). Depths in feet on the *y*-axis, orientation from north on the *x*-axis. Black holes are borehole breakouts oriented north–south (E symbols). Note also that the vertical and horizontal scales on the images are not 1:1, elongating the breakouts. White lines are bedding; black lines are synthetic deformation bands or zones; and dashed lines are antithetic deformation bands. Cloudy fluid that has cuttings flour in it is pale. (a) At the top of the fault, this cloudy fluid is replaced by clear water coming into the borehole from the breakouts. More clean fluid is coming into the borehole along deformation bands further up the hole. Near the base of the fault (b), clean fluids are coming in from the breakouts along deformation bands at the bottom center and top left and right of the image.

to unusually shaped grains in thin section. These observations show that fluid has, at some time, flowed in the fault core despite its present-day low porosity and permeability.

Fluid flow associated with the Big Hole fault is observed on downhole video image logs that were run in boreholes drilled through the fault (Figure 6). The throw on the fault at this location is 5 m (16 ft). On downhole video logs, the visual difference between cloudy fluids with suspended solids and clear groundwater fluids can be viewed directly. As seen in Figure 6b, the image below 199 ft (61 m) is cloudy, with static borehole fluids filled with drill-bit "flour," but clean fluids move out of the formation at the base of the fault, and the image clears up noticeably above this point. It appears that the fluid is moving into the borehole along a bedding surface intersecting the well just above the fault core, but further fluid moves into the borehole from the base of the fault. Figure 6a, by comparison, shows a plume or column of cloudy material moving into the borehole from the top of the fault, at about 190 ft (58 m); other plumes also emanate from within the fault zone. Thus, the groundwater flow in the area is strongly impacted by both the highly permeable slip surfaces and the impermeable fault core.

FAULT CORE THICKNESS MEASUREMENTS

To characterize variations in fault core thickness along the strike of the fault, a tape was laid parallel to the fault surface, and the thickness of the fault core was measured at 30-cm (12-in.) intervals with 457 measurements in total. The number of slip surfaces in the fault core was also collected at each 30-cm (12-in.) step. These measurements were made at six outcrops along the fault strike at locations with increasing displacement (Table 1). This allows us to determine the relationship between fault core thickness variations and displacement. If more than one slip-surface strand occurs at an outcrop, the fault core thickness was measured along all strands.

Fault core thickness is highly variable (Figure 7). Along a single fault strand, the thickness can range from almost zero to 20 or 30 cm (8 or 12 in.) within a few meters (Figure 3a). The maximum thickness is typically 15–20 cm (6–8 in.) but can be as high as 36 cm (14 in.) (location BHF24). The average fault core thickness across all sites was 6.1 cm (2.4 in.), with a standard deviation of 5.5 cm (2.2 in.). The highest average fault core thickness at an individual site is seen at BHF24 (Figure 7). At

Table 1. Summary of the fault core thickness data, locations given in order of distance along the Big Hole fault from the eastern fault tip (Figure 1). The total length of transects at each location includes the length of multiple strands. The standard deviation of the average thickness values is given in parentheses.

	Main Fault Offset (m)	*Outcrop Style*	*Total Transect Length (m)/ Number of strands*	*Number of Thickness Measurements*	*Average Fault Core Thickness (cm)*	*Maximum Fault Core Thickness (cm)*
BHF8	8.4	cliff	12.9:2	46	4.75 (2.75)	14
BHF17a	16.5 (<3)	base of wash	24.9:1	81	6.15 (5.42)	23
BHF17b	16.5 (>14)	base of wash	60.9:8	220	4.45 (3.93)	21
BHF20	19.9	base of wash	14.1:1	45	6.34 (4.23)	15
BHF24	23.9	inclined 30–45°	17.4:2	55	13.59 (5.53)	36
BHF23	23.0	cliff 45–90°	1.0:1	10	2.89 (1.87)	5.5

this outcrop, the fault core is composed of a yellow or pink poorly indurated gouge. It is not clear if this change in fault core character is related to the nature of the exposure (inclined slope, prone to weathering) or to the nature of the host rock (i.e., different eolian subfacies or proximity to the subaerial unconformity at the top of the Navajo Sandstone). Alternatively, it could be caused by a change in fault zone processes at higher displacements of the fault. However, the BHF23 outcrop, which has an almost equivalent amount of slip and which is at the base of a cliff almost directly below the BHF24 outcrop, contains the regular resistant fault core material.

Neither the maximum nor the average fault core thickness at each location correlates with the displacement on the fault (Figure 7). The BHF17 outcrop has two strands, and the total offset is partitioned on the two strands in such a way that the northern strand (BHF17a) has more than 3 m (10 ft) of throw, and the southern strand (BHF17b) has less than 14 m (46 ft) of throw (Figure 7). If these two sites are plotted as if both strands had 16.45 m (53.96 ft) of throw (with no account for the offset partitioning), the correlation between throw and average fault core thickness would be even less significant.

The fault core thickness frequency plot for the data from all locations (Figure 8a) shows a left-skewed distribution with a peak at 5-cm (2-in.) thickness. With the exception of BHF24, plots for each location (Figure 8b) show a similar left-skewed distribution, even where many substrands were measured (location BHF17b). No consistent change is present in fault core thickness frequency distribution with displacement. The largest number of thicker fault cores is seen at localities with both the highest and lowest displacement. Fault core thickness also does not correlate with the number of slip surfaces seen in the fault core (Figure 9). Where several strands to the fault zone exist, subsidiary strands (i.e., not the main throughgoing strand) can have locations where fault core exists as much as 9.5 cm (3.7 in.) thick but with no slip surface.

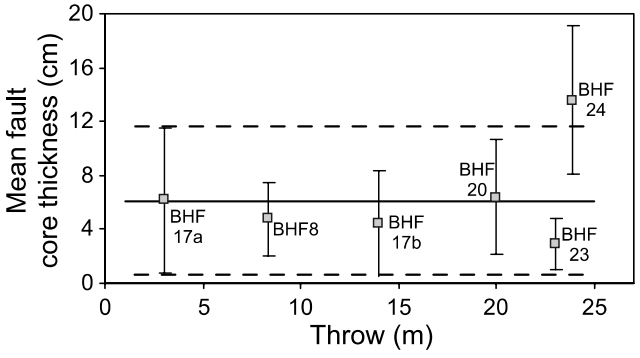

FIGURE 7. Mean fault core thickness vs. fault throw. The bars represent one standard deviation. The heavy line is the average for the entire data set, and the stippled lines are one standard deviation. No consistent change of mean fault core thickness occurred with increasing throw.

DISCUSSION

Evolution of Fault Core and Slip Surfaces: Preliminary Model

The model for the initiation of slip surfaces put forward by Aydin and Johnson (1978) did not distinguish whether the increased amount of crushing around slip surfaces was a precursor to slip-surface formation or occurred as displacement was accumulated (Figure 10a). The observations of fault core and slip-surface geometry presented here suggest that, for the Big Hole fault, a network of deformation bands does develop prior to the accumulation of slip on individual slip surfaces, and that localized intense grain crushing occurs before the nucleation of slip surfaces (Figure 10b). The

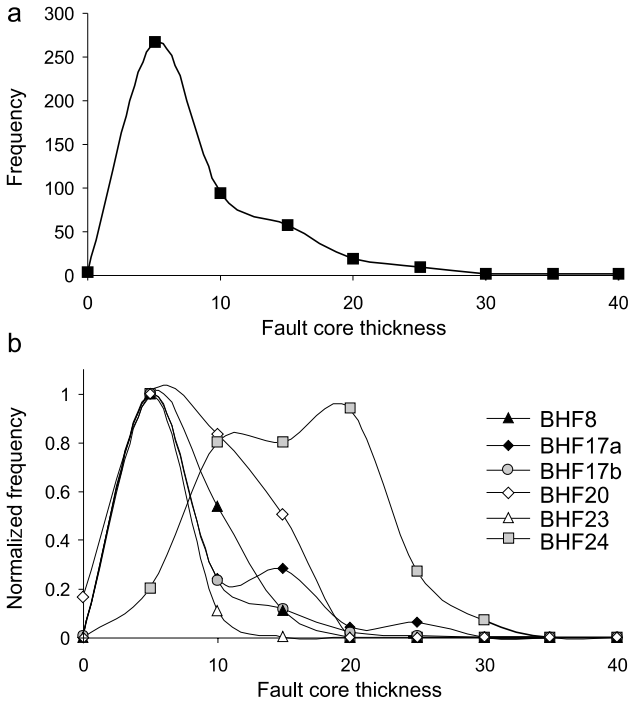

FIGURE 8. Fault core thickness frequency plots. (a) Global fault core thickness frequency plot showing a skewed distribution; (b) normalized fault core thickness frequency curves for each locality.

contrast in material properties between the highly comminuted fault core and host rock helps to localize slip surfaces at the boundaries of the low-porosity and, hence, denser fault core zone (Figure 10c). The main slip surface is always throughgoing, but on slip surfaces away from main faults, there can be gaps where no surfaces are present but where fault corelike material is developed (Figure 10d). However, the fault core continues to develop after localization of a throughgoing slip surface.

The critical parameters for the nucleation of slip surfaces have not been ascertained but could include critical strain, number of deformation bands, deformation-band zone thickness, and setting along the fault. The change of deformation mechanisms from grain rolling and crushing in zones of deformation bands to brittle fracture in the fault core is likely to be controlled by the drastic reduction in porosity in the fault core (Shipton and Cowie, 2001). Faults that form in low-porosity sandstones deform by brittle fracturing without grain rolling (Anders and Wiltschko, 1994; Vermilye and Scholz, 1998; Steen and Andresen, 1999), and this is also the case for continued deformation in the fault core material. This change in deformation mechanism results in a change of permeability, with the deformation of high-porosity host rock reducing permeabilities and the deformation of low-porosity rock (fault core) enhancing permeabilities (microfractures). Note that along the Big Hole fault, more than one of these mechanisms could be active at the same time.

Fault core is locally thicker where kinematic incompatibilities occur at intersections between slip surfaces (Figure 10b). In cross section, triangular areas of the fault core are localized at junctions of synthetic and antithetic slip surfaces or deformation-band clusters. In plan view, elongate lozenge-shaped pods of fault core occur along the main slip surfaces, suggesting that the synthetic and antithetic slip surfaces are not entirely strike parallel and have some curvature or corrugation. Antonellini and Aydin (1995) and Tindall and Davis (1999) show that deformation-band faults typically have thick zones of deformation bands at stepovers between fault segments. The thickness variations observed here may reflect some of these early-formed variations in fault structure (e.g., Figures 5c, 10b).

These observations emphasize the three-dimensional nature of the network of slip surfaces and show that predicting the thickness of fault core and, therefore, permeability at an individual location is complex. The thickness distribution of the fault core at the Big Hole fault is independent of the displacement on the main fault and the number of slip surfaces. The frequency of deformation bands and the number of slip surfaces are also independent of displacement. The width of the entire damage zone does seem to scale with displacement at the Big Hole fault (Shipton and Cowie, 2001) and at other deformation-band faults (Knott et al., 1996; Beach et al., 1997, 1999; Myers, 2004; Fossen and Hesthammer, 2000). Antonellini and Aydin (1995) demonstrated that a difference in microstructures exists between deformation bands in different host rocks; it is unclear to what extent this is true for slip surfaces and fault core. Local stress conditions, deformation history, and host rock variation should be considered when investigating the geometry and scaling of damage zones and fault core around deformation-band faults.

The Effect of the Fault Core on Single-phase Fluid Flow

The effect that a fault-related reduction of porosity and permeability has on fluid flow depends on the number of fluid phases in the rock. Reservoir simulators that incorporate faults either assign flow properties to a series of elements that represent the faults or, more commonly, have the fault modeled as a surface between two grid blocks and assign a single flow property value to the surface. By averaging material properties of the fault rock that affect the flow of either single- or two-phase flow, we can calculate an effective property that is constant on the scale of an individual grid block (Manzocchi et al., 2002).

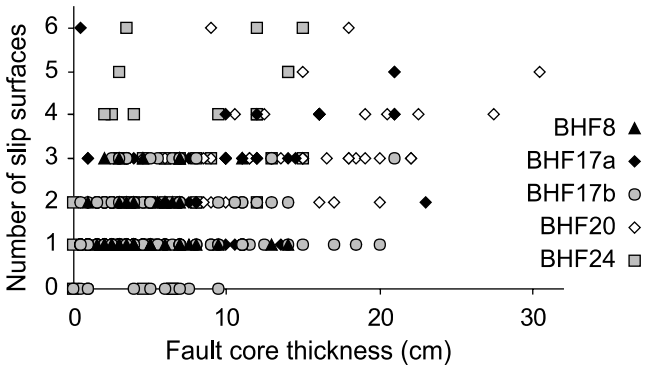

FIGURE 9. Fault core thickness vs. number of slip surfaces in or around the fault core. Each symbol represents data from a different outcrop. No correlation of fault core thickness with number of slip surfaces is present.

In single-phase flow (equivalent to flow through saturated rock [Manzocchi et al., 2002]), the controlling parameters are fault rock permeability, k_f, and fault thickness, t_f. Flow simulations commonly use a transmissibility multiplier, T, to represent the effect of fault rock on fluid flow between two grid blocks relative to host rock grid block permeabilities. Manzocchi et al. (1999) showed that for the case where grid blocks adjacent to the fault are the same size, L, and the matrix permeability of the grid blocks on either side of the fault, k_m, is the same, T is a function of fault thickness, t_f, and permeability, k_f, such that

$$\frac{1}{T} = 1 + \frac{t_f}{L}\left(\frac{k_m - k_f}{k_f}\right) \quad (1)$$

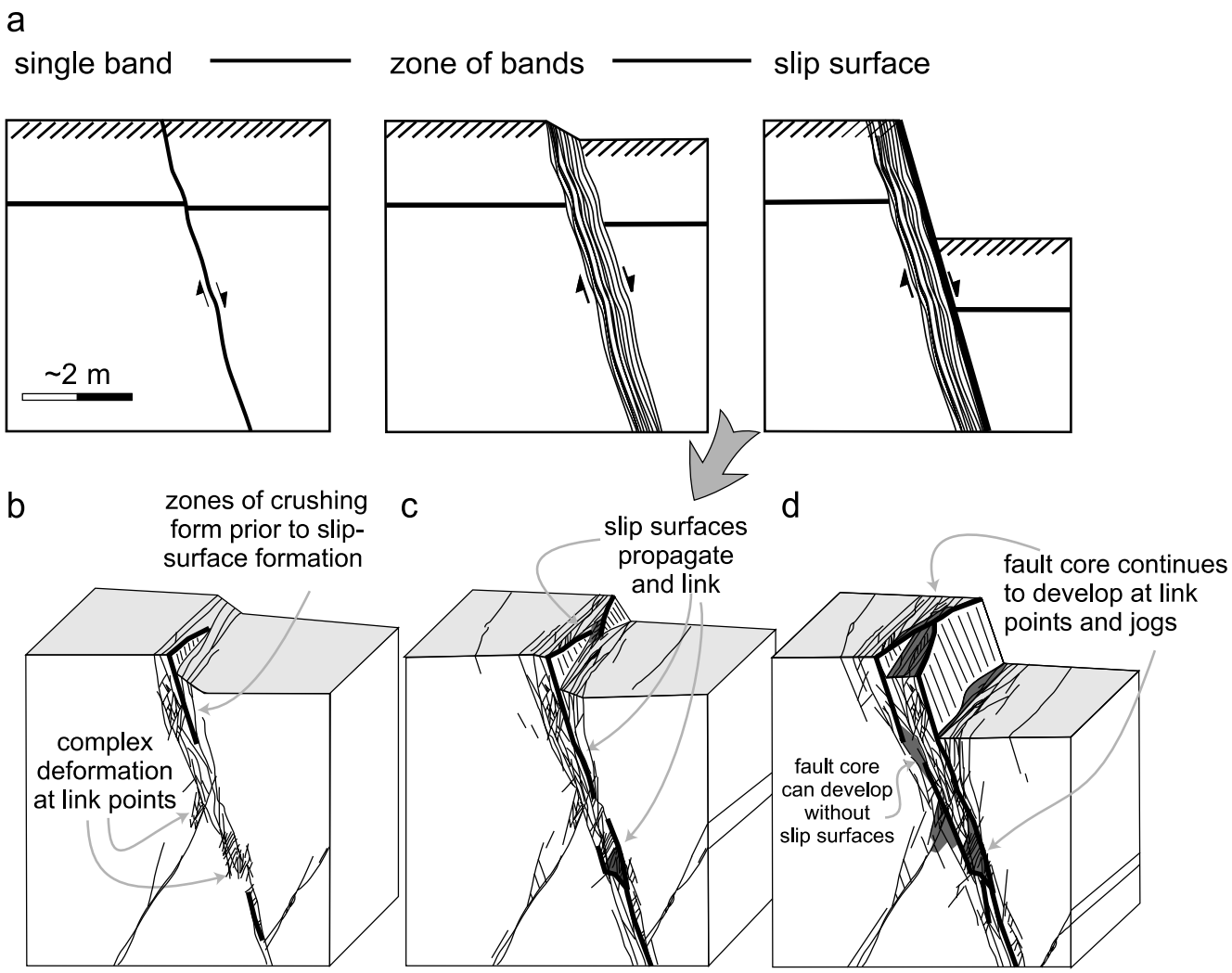

FIGURE 10. (a) Model of Aydin and Johnson (1978) modified to show development of slip surface and fault core. (b) Slip surfaces nucleate at local points of high-intensity grain crushing. (c) Slip surface segments propagate through developing zone of bands to link and eventually form throughgoing surface. (d) As displacement increases along a hroughgoing slip surface, further development is focused at kinematically incompatible linkage points. A thin veneer of highly comminuted fault core material lines each of the slip surfaces but is too narrow to be represented on these figures.

If we neglect the effect of faults in the damage zone, we can use this equation to examine the sensitivity of T to fault core thickness along the Big Hole fault. Damsleth et al. (1998), in a study of the effect of subseismic faults in the Njord field, Norway, calculated that faults with T values of less than 0.0005 have a sealing effect. If we use host rock permeability of 600 md (Shipton et al., 2002), fault core permeability of 0.007 md (Antonellini and Aydin, 1994), and an arbitrary grid block length of 15 m (49 ft) (see Shipton et al., 2002, for the effect of varying grid block size), then $T = 0.0005$ corresponds to fault core thicknesses above 35 cm (14 in.), close to the maximum thickness we measured. However, if the fault permeability is as low as 0.0001 md, or if host rock permeability was as high as 4000 md, the critical sealing thickness would be 5 cm (2 in.), close to the average measured fault core thickness.

This approach assumes a constant fault core thickness at the grid block scale; however, the along-strike variability of the fault core thickness is pronounced from meter to millimeter scales. The majority of reservoir simulators are not able to represent such fine-scale variability and rely on upscaling to simplify the transmissibility structure of the fault. Manzocchi et al. (1999) suggest that for situations where adjacent grid blocks have the same host rock and fault zone permeabilities, the area-weighted harmonic average of fault zone thickness (t_f) can be used in calculations of transmissibility multipliers, such that

$$t_f = A\left[\sum_{n=1}^{n=i} \frac{A_i}{t_{fi}}\right]^{-1} \quad (2)$$

where A is the total area of the fault surface, which is divided into sub-areas (A_i) with fault thickness (t_{fi}).

We calculate the area-weighted harmonic average of fault zone thickness for our data by assuming a unit depth of fault surface (the length-weighted harmonic average). The harmonic average is then used to calculate transmissibility for each location along the Big Hole fault (Table 2). This analysis shows that if the geometry of deformation bands around the main fault provides a pathway for fluid flow to the fault core, then a fault that juxtaposes sand against sand is unlikely to retard single-phase flow across the fault surface.

For deformation-band faults in high-permeability host rocks, the along-strike geometry and thickness variations of the fault core become important in determining if a fault acts as a seal. A low fault core thickness "hole" in an otherwise sealing fault core could provide a pathway for fluid flow through the fault. From our model of fault core development at the location of linkage between both coplanar and antithetic fault segments, we might expect the number of holes along a fault surface to decrease if the number of antithetic fault strands increases around higher displacement faults. It is of particular importance to quantify any scaling of fault permeability with offset at sand-sand juxtapositions, because this is commonly presumed by both geologists and reservoir engineers (Heinemann et al., 1998; Manzocchi et al., 1999).

The Effect of the Fault Core on Two-phase Fluid Flow

The main parameter controlling fault seal in two-phase flow systems is capillary entry pressure. Assuming that a fault is sealing by capillary pressure, the hydrocarbon column height that a fault can support, h, can be related to the radius of pore throats in the fault rocks, R, by

$$h = \frac{2\gamma}{Rg(\rho_w - \rho_c)} \quad (3)$$

where γ is the dynamic viscosity; ρ_w is the density of water; ρ_c is the density of oil; and g is gravitational acceleration. The empirical equations of Pittman (1992) can be used to estimate the pore-throat radius corresponding to the capillary entry pressures of fault rocks

Table 2. Calculated transmissibilities for each location along the Big Hole fault using the area-weighted harmonic average for the fault core thickness and assuming host rock grid blocks of 15-m (49-ft) length. The harmonic average is calculated for only the throughgoing strand at each location. Transmissibility is calculated for extreme values of host and fault permeability. The fault is assumed to leak if the transmissibility is more than 0.0005 (Damsleth et al., 1998).

	t (cm)	*T (k_m = 600; k_f = 0.007)*		*T (k_m = 600, k_f = 0.001)*		*T (k_m = 3000, k_f = 0.007)*	
BH8	1.91	0.0091	leak	0.0013	leak	0.0022	leak
BH17a	2.86	0.0061	leak	0.0009	leak	0.0015	leak
BH17b	3.16	0.0055	leak	0.0008	leak	0.0013	leak
BH20	7.00	0.0025	leak	0.0004	*seal*	0.0006	leak
BH24	9.71	0.0018	leak	0.0003	*seal*	0.0004	*seal*
BH23	1.23	0.0141	leak	0.0020	leak	0.0034	leak

based on their porosities and permeabilities. Using porosities of the fault core between 1 and 5% (Shipton and Cowie, 2001) and permeability of 0.007 md (Antonellini and Aydin, 1994), we calculate the pore aperture radius corresponding to the displacement pressure as 0.24–0.13 μm. These values correspond to hydrocarbon column heights of 103–191 m, respectively.

Data on the two-phase petrophysical properties of deformation-band faults are sparse. Gibson (1998) and Ogilvie and Glover (2001) measured values of R between 0.18 and 13.3 μm, corresponding to hydrocarbon column heights of 137 and 2 m, respectively. Knott (1993) found that 30% of sand-sand juxtapositions formed a seal in the North Sea. The hydrocarbon column heights measured by Gibson (1994) were approximately proportional to fault throw for sand-sand juxtapositions, with throws as much as 75 m (246 ft) (his figure 6), suggesting a relationship between fault offset and the sealing potential of the faults. These data suggest that deformation-band faults can be a barrier to two-phase fluid flow in hydrocarbon reservoirs, but that the petrophysical properties of the fault core are variable. Our data show that all slip surfaces are surrounded by a poorly sorted, fine-grained (and, therefore, small pore-throat size) fault core. Even if its thickness is very small, this should provide a capillary seal to two-phase flow. There does not seem to be an increase in grain crushing (producing a decrease in pore-throat size) with accommodation of slip, and there is some evidence for brittle fracture of the fault core occurring with increased slip, which would drastically decrease the sealing capacity of the fault zones. Further studies of the grain size distribution, pore-throat size, and capillary entry pressure of fault core material are necessary to fully quantify two-phase flow parameters for faults in sandstone.

The above analyses show that if a fluid pathway to the fault core exists through the damage zone, and the fault core contains open holes with little or no fault core material along them, then a fault that juxtaposes sand against sand is unlikely to significantly retard flow across the fault surface. Faults in the North Sea have a diagenetic component that helps them seal, but minimal diagenesis is present along the Big Hole fault. Much more petrophysical data need to be collected from deformation-band faults, and ideally, these data should be calibrated to cross-fault hydrocarbon column heights in reservoirs with known total hydrocarbon height (Fisher and Knipe, 2001; Fisher et al., 2001).

Flow along Slip Surfaces

The presence of minimal cements in the fault core and the observation of flow along slip surfaces in the image logs (Figure 6) suggest that slip surfaces have been and, in places, continue to be high-permeability conduits for fluid flow along the fault surface. Matthai et al. (1998) in Arches National Park, Utah, and Steen and Andresen (1999) in west Greenland have also described slip surfaces in deformation-band faults that contain neoformed carbonate cement. Matthai et al. (1998) use these observations to justify very high permeability values for slip surfaces in their flow models. The actual permeability values that would be appropriate to use for slip surfaces in flow models will vary depending on a large number of factors that are likely to be site specific and include the aperture and tortuosity of the fracture, geometry and linkage of fracture segments, and orientation with respect to applied stress.

High-permeability slip surfaces in this study are always surrounded by low-permeability and high-inferred capillary entry pressure fault core. Therefore, they are likely to represent barriers to cross-fault fluid flow, unless the fault core material is breached by fractures that develop during continued slip on the fault, at which point they will act as flow conduits. The majority of slip surfaces run parallel to the fault, so the predominant effect of open slip surfaces will be to conduct fluid parallel to the fault. Slip surfaces commonly cut through the fault core in the Big Hole fault (Figure 4) and, therefore, may act as pathways for across-fault flow (Jourde et al., 2002).

CONCLUSIONS

The Big Hole fault, Utah, is a deformation-band fault consisting of a fault core, damage zone, and surrounding high-porosity host rock (Navajo Sandstone). Similar to other faults in this lithology, the primary brittle deformation structures are deformation bands that dominate the damage zone. The fault core consists of deformation bands that are very densely spaced and are characterized by highly crushed grains and very little remaining pore space. This fault core has a reduced grain size and wider grain size distribution than the host rock and will therefore have reduced permeabilities and pore-throat sizes.

Fault core is wider in places where deformation bands or slip surfaces link, forming pods that are triangular-shaped cross sections and lozenge-shaped in plan view. Because slip surfaces are discrete planes along which significant slip can occur, they may represent pathways for fluid flow in a fault zone that otherwise has a very low permeability because of the presence of deformation bands and fault core. Slip surfaces nucleate in small patches at a relatively early stage in the development of a zone of deformation bands at points where grain crushing is locally increased. They then propagate and link up to form an

anastomosing network. The development of fault core, the growth and linkage of slip surfaces in three dimensions, and the nature of these slip surfaces at depth (open or closed) have important implications for understanding the structural and permeability architecture of faults in this lithology. The Big Hole fault has relatively little diagenesis associated with it, and faults with only mechanical damage may be relatively poor seals compared with cemented cataclastic faults.

The thickness of the fault core is one of the primary controls on the bulk transverse permeability of these fault zones. Our data of fault core thickness along strike suggest that fault core thickness is highly variable, and that fault core thickness and thickness frequency distributions are not simply correlated to a single parameter, such as displacement or number of slip surfaces. Further work is necessary to understand the predictability of fault permeability with easily measurable parameters. To incorporate this fault zone element into accurate simulations of fault zone permeability, it is essential that a large database of fault core architecture and permeability properties be collected for faults in a given setting. Gathering data from several faults in different host rocks and fault displacements will maximize the usefulness of this database and allow any underlying relationships to be characterized fully.

ACKNOWLEDGMENTS

Comments from Jennifer Wilson, Rasoul Sorkhabi, and an anonymous reviewer substantially improved this chapter. Funding for this work was provided by the Office of Basic Energy Sciences–Department of Energy grants DE-FG03-00ER15042 and DE-FG03-95ER14526 and by Big Hole Drilling Project sponsors: ARCO and ARCO Alaska, Enterprise Oil, Exxon, Japan National Oil Corporation (presently Japan Oil, Gas and Metals National Corporation), Mobil, Schlumberger-Doll Research, Shell, and Statoil. Hoda Sondossi assisted in collecting the field data.

REFERENCES CITED

Anders, M. H., and D. V. Wiltschko, 1994, Microfracturing, palaeostress and the growth of faults: Journal of Structural Geology, v. 16, p. 795–815.

Antonellini, M., and A. Aydin, 1994, Effect of faulting on fluid flow in porous sandstones: Petrophysical properties: AAPG Bulletin, v. 78, p. 355–377.

Antonellini, M., and A. Aydin, 1995, Effect of faulting on fluid flow in porous sandstones: Geometry and spatial distribution: AAPG Bulletin, v. 79, p. 642–671.

Antonellini, M. A., A. Aydin, and L. Orr, 1999, Outcrop aided characterisation of a faulted hydrocarbon reservoir: Arroyo Grande oil field, California, U.S.A., *in* W. C. Haneberg, P. S. Mozley, C. J. Moore, and L. B. Goodwin, eds., Faults and subsurface fluid flow: American Geophysical Union Geophysical Monograph 113, p. 7–26.

Aydin, A., and A. M. Johnson, 1978, Development of faults as zones of deformation bands and as slip-surfaces in sandstones: Pure and Applied Geophysics, v. 116, p. 931–942.

Beach, A., J. L. Brown, A. L. Welbon, J. E. McCallum, P. Brockbank, and S. Knott, 1997, Characteristics of fault zones in sandstones from NW England: Application to fault transmissibility, *in* N. S. Meadows, S. P. Trueblood, M. Hardman, and G. Cowan, eds., Petroleum geology of the Irish Sea and adjacent areas: Geological Society (London) Special Publication 124, p. 315–324.

Beach, A., A. I. Welbon, P. J. Brockbank, and J. E. McCallum, 1999, Reservoir damage around faults: Outcrop examples from the Suez Rift: Petroleum Geoscience, v. 5, p. 109–116.

Damsleth, E., V. Sanglot, and G. Aamodt, 1998, Subseismic faults can seriously affect fluid flown in the Njord field off western Norway— A stochastic fault modelling case study: Presented at the Society of Petroleum Engineers Annual Technical Conference and Exhibition, New Orleans, September 27–30: SPE Paper 49024, 10 p.

Edwards, H. E., A. D. Becker, and J. A. Howell, 1993, Compartmentalization of an aeolian sandstone by structural heterogeneities: Permo-Triassic Hopeman Sandstone, Moray Firth, Scotland, *in* C. P. North and D. J. Prosser, eds., Characterization of fluvial and aeolian reservoirs: Geological Society (London) Special Publication 73, p. 339–365.

Fisher, Q. J., and R. J. Knipe, 1998, Fault sealing processes in siliciclastic sediments, *in* G. Jones, Q. J. Fisher, and R. J. Knipe, eds., Faulting, fault sealing, and fluid flow in hydrocarbon reservoirs: Geological Society (London) Special Publication 147, p. 117–133.

Fisher, Q. J., and R. J. Knipe, 2001, The permeability of faults in siliciclastic petroleum reservoirs of the North Sea and Norwegian continental shelf: Marine and Petroleum Geology, v. 18, p. 1063–1081.

Fisher, Q. J., S. D. Harris, E. McAllister, R. J. Knipe, and A. J. Bolton, 2001, Hydrocarbon flow across faults by capillary leakage revisited: Marine and Petroleum Geology, v. 18, p. 251–257.

Flodin, E. A., L. J. Durlofsky, and A. Aydin, 2004, Upscaled models of flow and transport in faulted sandstone: Boundary condition effects and explicit fracture modelling: Petroleum Geoscience, v. 10, p. 173–181.

Fossen, H., and J. Hesthammer, 2000, Possible absence of small faults in the Gullfaks field, northern North Sea: Implications for downscaling of faults in some porous sandstones: Journal of Structural Geology, v. 22, p. 851–863.

Gibson, R. G., 1994, Fault-zone seals in siliciclastic strata of the Columbus basin, offshore Trinidad: AAPG Bulletin, v. 78, p. 1372–1385.

Gibson, R. G., 1998, Physical character and fluid-flow

properties of sandstone-derived fault zones, *in* M. P. Coward, T. S. Daltaban, and H. Johnson, eds., Structural geology in reservoir characterization: Geological Society (London) Special Publication 127, p. 83–97.

Heinemann, Z. E., G. F. Heinemann, and B. M. Tranta, 1998, Modeling heavily faulted reservoirs: Presented at the Society of Petroleum Engineers annual technical conference and exhibition, New Orleans, September 27–30: SPE Paper 48998, 11 p.

Hesthammer, J., T. E. S. Johansen, and L. Watts, 2000, Spatial relations within fault damage zones in sandstone: Marine and Petroleum Geology, v. 17, p. 873–893.

Hood, J. W., and D. J. Patterson, 1984, Bedrock aquifers in the northern San Rafael Swell area, Utah, with special emphasis on the Navajo Sandstone: State of Utah Department of Natural Resources Technical Publication No. 78, 128 p.

Jourde, H., E. A. Flodin, A. Aydin, L. J. Durlofsky, and X. Wen, 2002, Computing permeabilities of fault zones in eolian sandstone from outcrop measurements: AAPG Bulletin, v. 86, p. 1187–1200.

Knott, S. D., 1993, Fault seal analysis in the North Sea: AAPG Bulletin, v. 77, p. 778–792.

Knott, S. D., A. Beach, P. J. Brockbank, J. L. Brown, J. E. McCallum, and A. I. Welbon, 1996, Spatial and mechanical controls on normal fault populations: Journal of Structural Geology, v. 18, p. 359–372.

Krantz, R. W., 1988, Multiple fault sets and three-dimensional strain: Theory and application: Journal of Structural Geology, v. 10, p. 225–237.

Mair, K., I. Main, and S. Elphick, 2000, Sequential growth of deformation bands in the laboratory: Journal of Structural Geology, v. 22, p. 25–42.

Manzocchi, T., J. J. Walsh, P. Nell, and G. Yielding, 1999, Fault transmissibility multipliers for flow simulation models: Petroleum Geoscience, v. 5, p. 53–63.

Manzocchi T., A. E. Heath, J. J. Walsh, and C. Childs, 2002, The representation of two phase fault-rock properties in flow simulation models: Petroleum Geoscience, v. 8, p. 119–132.

Matthai, S. K., A. Aydin, D. D. Pollard, and S. G. Roberts, 1998. Numerical simulation of departures from radial drawdown in a faulted sandstone reservoir with joints and deformation bands, *in* G. Jones, Q. J. Fisher, and R. J. Knipe, eds., Faulting, fault sealing and fluid flow in hydrocarbon reservoirs: Geological Society (London) Special Publication 147, p. 157–191.

Myers, R., and A. Aydin, 2004, The evolution of faults formed by shearing across joint zones in sandstone: Journal of Structural Geology, v. 26, p. 947–966.

Ogilvie, S. R., and P. W. J. Glover, 2001, The petrophysical properties of deformation bands in relation to their microstructure: Earth and Planetary Science Letters, v. 193, p. 129–142.

Pittman, E. D., 1981, Effect of fault-related granulation on porosity and permeability of quartz sandstones, Simpson Group (Ordovician) Oklahoma: AAPG Bulletin, v. 65, p. 2381–2387.

Pittman, E. D., 1992, Relationship of porosity and permeability to various parameters derived from mercury injection-capillary pressure curves for sandstone: AAPG Bulletin, v. 76, p. 191–198.

Shipton, Z. K., and P. A. Cowie, 2001, Damage zone and slip-surface evolution over μm to km scales in high-porosity Navajo Sandstone, Utah: Journal of Structural Geology, v. 23, p. 1825–1844.

Shipton, Z. K., J. P. Evans, K. Robeson, C. B. Forster, and S. Snelgrove, 2002, Structural heterogeneity and permeability in faulted eolian sandstone: Implications for subsurface modelling of faults: AAPG Bulletin, v. 86, p. 863–883.

Steen, Ø., and A. Andresen, 1999, Effects of lithology on geometry and scaling of small faults in Triassic sandstones, east Greenland: Journal of Structural Geology, v. 21, p. 1351–1368.

Tindall, S. E., and G. H. Davis, 1999, Monocline development by oblique-slip fault-propagation folding: The east Kaibab monocline, Colorado Plateau, Utah: Journal of Structural Geology, v. 21, p. 1303–1320.

Vermilye, J. M., and C. H. Scholz, 1998, The process zone: A microstructural view: Journal of Geophysical Research, v. 103, p. 12,223–12,237.

Walsh, J. J., J. Watterson, A. E. Heath, and C. Childs, 1998, Representation and scaling of faults in fluid flow models: Petroleum Geoscience, v. 4, p. 241–251.

Yielding, G., B. Freeman, and D. T. Needham, 1997, Quantitative fault seal prediction: AAPG Bulletin, v. 81, p. 897–917.